ELSEVIER

Atmospheric Research 89 (2008) 194–205

ATMOSPHERIC RESEARCH

www.elsevier.com/locate/atmos

Ground-based remote sensing of aerosol optical properties in one city in Northwest China

Jianjun Liu [a], Youfei Zheng [a,*], Zhanqing Li [b], Rongjun Wu [a]

[a] College of Environmental Science and Engineering, Nanjing University of Information Science & Technology, Nanjing 210044, China
[b] Department of Atmospheric & Oceanic Science, University of Maryland, College Park, MD 20782, USA

Received 14 July 2007; received in revised form 7 November 2007; accepted 28 January 2008

Abstract

A ground-based sky radiometer was used to measure direct and scattering solar irradiances, as well as aureole radiances, from October 2003 to August 2004 over Yinchuan, China. The aerosol particles optical depth (AOD), Angstrom exponent (ALPHA), volume size distributions, refraction index and single scattering albedo of aerosols were simultaneously retrieved using the 'SKYRAD' code. The results reveal that during the study period, the AOD varied seasonally, with a vernal maximum and a winter minimum, and the variation in ALPHA was opposite, with a vernal minimum and a winter maximum. The diurnal variability of AOD was significant, showed a similar variation pattern in spring, summer and autumn and had another variation pattern in winter. The frequency distributions of AOD and ALPHA approximately follow a log-normal probability distribution and a normal probability distribution, respectively. The relationship between ALPHA and AOD showed a simple dependence of ALPHA on AOD in spring and can be characterized by one integrated exponential function. And no clear relationship between AOD and ALPHA was evident in other seasons.

The aerosol volume size distributions can be characterized by the sum of two log-normal distributions, and represented an accumulation mode with a radius of about 0.15 μm, and a coarse mode with a radius of about 7 μm, which was the main aerosol mode in this area. The real parts of the refraction index rose in spring, and exhibited a low sensitivity to wavelengths; the imaginary parts of the refractive index decreased noticeably in spring and also showed a low sensitivity to wavelength. Both their low sensitivities to wavelengths slightly varied with time, but no clear patterns were found. The aerosol single scattering albedo in spring was much higher than in other seasons, and increased dramatically with increase in wavelength, from 0.92 at 400 nm to 0.97 at 1020 nm. In other seasons, it showed a slightly decreased with wavelength. The aerosol direct radiative forcing efficiency at the short wavelength is −55.31, −59.71, −60.13 and −60.38 at surface and 13.89, 10.39, 2.30 and 2.64 at TOA in spring, summer, autumn and winter, respectively. The value at surface/TOA in spring is lower/higher than that in other seasons, indicating the influence of the dust aerosol.

Keywords: Aerosol; Optical properties; Radiative forcing; Sky radiometer; Yinchuan

1. Introduction

Aerosols comprise one important component of the Earth–atmosphere system, which influences radiative transfer in the atmosphere and plays an extremely important role both in global climatic change and in the

* Corresponding author. College of Environmental Science and Engineering, Nanjing University of Information Science & Technology, No.114, Pangcheng New Street, PuKou District, Nanjing 210044, China. Tel.: +86 25 58731433.
E-mail addresses: jianjun5212@hotmail.com (J. Liu), zhengyf@nuist.edu.cn (Y. Zheng).

0169-8095/$ - see front matter © 2008 Published by Elsevier B.V.
doi:10.1016/j.atmosres.2008.01.010

biogeochemical cycle. Many studies regarding the retrieval of aerosol particles optical properties, their character of spatial and temporal variations, and their influence on atmospheric radiation and climate have been carried out (Mao, 2006; Xin et al., 2007; Wang et al., 2004; Chen et al., 2005; Kaufman et al., 2002; Dubovik et al., 2002; Osborne et al., 2004; Bates et al., 2006; Kelly et al., 2007). However, these aerosol effects still contain considerable uncertainties due to the poor understanding of aerosol properties and their spatial and temporal variation (IPCC, 2001, 2007) and aerosol continue to play a crucial role in current assessments and predictions of global climate (Hansen et al., 2000).

Ground-based remote sensing of aerosols is ideal for the reliably and continuously derivation of aerosol particles properties in key locations around the world and more information than can be obtained from space-borne remote sensing, with no background signal ground-based AOD though is more reliable. It always delivers effective values, representative for the entire vertical column with no height dependence and is particularly true for the refractive indices and the size distribution parameters of the particle size distribution. Validating aerosol products obtained from various satellite sensors may need ground-based measurements of a variety of optical aerosol characteristics with different data quality requirements. Many aerosol ground-based observation networks have been established in order to understand the optical properties and indirectly evaluate their effect on climate, including AERONET (An Automatic Robotic Sun and Sky Scanning Measurement Program) (Holben et al., 1998, 2001), SKYNET (A Sun and Sky Radiometer Network Based in East-Asia) (Takamura et al., 2002), and GAW (Global Atmosphere Watch Programme) (WMO, 2001).

It is well understood that aerosols are not well-mixed in the atmosphere hence aerosol particles properties, such as the optical depth (AOD), the Angstrom exponent (ALPHA) and others would depend on location scenarios that govern emission, transport, atmospheric transformation and removal of aerosol particles. Given the short lifetime of aerosol particles, their properties vary with time and from one region to another. Yinchuan is located at the northwest of Ningxia province of China, which is a typical semiarid area near by desert and Gobi. The annual averaged rainfall here is 200 mm and the annual average of temperature is 8.5 °C and with huge annual and daily difference. The monthly average of wind speed is about 2 m/s, with large values occurred in spring. So, it is frequently affected by dust storms, especially in spring. But, due to the influence of the mountain, located at west of it, the effects of dust are less serious than that in some other sites in northwest China, such as Dunhuang sites. Meanwhile, as the most cities in north China, it is also a city with high industrial pollution. So the aerosol particles properties over this area are good representative for the most regions in northwest China. Due to its special location and good infrastructure, Yinchuan has been established as one of the super-sites for many international aerosol field experiments, such as, China and Japan joint plan on Aeolian dust effect on climate (ADEC).

The objective of this study is to simultaneously retrieve aerosol particles optical depth, Angstrom exponent, size distribution, single scattering albedo, as well as the real and imaginary parts of the refractive index over Yinchuan area through using of direct and scattering solar irradiances, as well as aureole radiances (the region of enhanced brightness that surrounds the solar disk in cloudless conditions and is mainly due to the forward single scattering of light by the aerosol particles) from a sky radiometer. The characterization of the climatology of these aerosol particles optical properties is discussed and the aerosol direct radiative effects are also estimated, which will sever to improve current knowledge about aerosols in this area and around the world. The paper is organized as follows. After a brief description of instrumentation and data in the next section, Section 3 provides the methodology of treating data, Section 4 describes the aerosol optical properties (AOD, ALPHA, size distribution, etc.) and direct radiative forcing efficiency. Our simple summaries are presented in Section 5.

2. Instrumentation and data

2.1. Instrument and calibration

The ground-based sky radiometer (POM-01; manufactured by Prede Co., Ltd., Tokyo, Japan) is a convenient, portable instrument that can measure direct and scattering solar irradiances, as well as the aureole in the solar almucantar and the principal plane, in daytime under clear skies. It consists of seven filters with the central wavelengths at 315, 400, 500, 675, 870, 940, and 1020 nm; the half-bandwidth wavelength at 315 nm is 3 nm and less than 10 nm at the other wavelengths. Measurements made at 315 and 940 nm are used for deriving the O_3 concentration and precipitable water column amount, respectively; measurements at the other wavelengths are used for aerosol remote sensing. The field of view is 1° and the minimum angle for sky measurements is about 3°. The photometer is mounted on a vertical–horizontal two-axis mount that is driven by digital servomotors to carry out sky radiance almucantar measurements. A preprogrammed sequence

of measurements is taken by the aureolemeter: during periods when the air mass is larger than 3, solar direct and scattering measurements are made at about 0.25 air mass intervals, while at smaller air masses, the sampling interval is typically 10 min. Details of the scanning method can be found in Tonna et al. (1995).

Accurate calibrate of the radiometer constant, $F_{0,\lambda}$ is essential in ground-based measurements (Schmid et al., 1998). The accuracy with which AOD can be retrieved depends mainly on the accuracy of the $F_{0,\lambda}$ value. $F_{0,\lambda}$ errors should be less than 2% in order to obtain AOD with an uncertainty less than 0.02 when the air mass is equal to 1. The Langley method (LM), a straightforward application of the Bouguer–Lamber–Beer law, is practically the de facto standard, owing to its high accuracy and its convenient application in the field. But the assumption that the atmosphere remains stable during the calibration period of one to several hours, is not satisfied at most locations and under most situations. Accordingly, some modified Langley methods (MLMs) have been developed (Tanaka et al., 1986; O'Neill, 1984), in which temporarily variable atmospheric turbidity is taken into consideration. In this paper, the radiometer was calibrated using the modified Langley method suggested by Nakajima et al. (1996), which is an extension of the Tanaka's MLM. The first step involves performing an inversion with only forward scattering intensity data (3°–40°), form which temporarily variable aerosol optical depth (AOD) are derived. There are two reasons for only considering the forward scattering. One reason is that the forward scattering part (3°–40°) is mainly consisting of the diffracted radiation which is mostly dependent on the scattering cross section of particles without much dependence on the refractive index (especially imaginary index) and non-sphericity. Another is that this part is just circum-solar region which tends not to be affected by inhomogeneity of the horizontal aerosol distribution and ozone absorption etc. These AOD values are then multiplied by the corresponding air mass (m) and used to obtain the radiometer constant ($F0$) through the Lambert Beer's equation: $\ln(F)=\ln(F0)-m*\mathrm{AOD}$. In this process, AOD can be a rough estimate of atmospheric turbidity which includes the temporal change during the Langley plot. And this method is not affected by such temporal change of AOD through using an AOD with a temporal change included, even if it is a rough estimate. A sensitivity study showed that the effects of the uncertainties in the input parameters, such as refractive index, and measurement errors on calibration were weak, so a calibration accuracy of 1% can be achieved by this method. Hence, the errors in AOD retrievals are approximately 0.01 at one air mass.

2.2. Data

Direct and scattering solar irradiance measurements, as well as aureole radiance measurements, were taken at the Yinchuan observation station (Latitude: 106.21°E; Longitude: 38.48°N; Altitude: 1111 m). The sampling interval is 10 min from sun rises to sun sets under clear skies. And the observation period was from October 2003 to August 2004. Due to the malfunction of radiometer, the data of September were missed. Surface pressures needed for Rayleigh scattering optical depth calculations were obtained from the Yinchuan meteorological observatory located near the observation station. The columnar ozone contents for ozone absorption optical depth calculations were obtained from the Total Ozone Mapping Spectrometer. The surface albedos over Yinchuan area were obtained from the MODIS surface albedo products.

3. Methodology

Aerosol properties were retrieved using the newest version (v4.2, April 2006) of the 'SKYRAD' code, which was developed by Nakajima et al. (1996). The code consists of two programs: the first is for computing simulated direct and diffuse solar radiation, which is for making a test simulation data for the inversion code and returns the simulated spectral angular distribution of sky radiance and direct solar irradiance into the variable AUR for each angle (0 means direct) and wavelength. And the second is for retrieving aerosol properties from solar radiation data (real or simulated). In this code, the input data mainly consist of the solar zenith angle and geometry (almucantar, principal plane), the number and value of wavelengths and scattering angles, the calibrated radiometer constant of radiometer, the surface pressures, the ozone contents, the surface albedos, latitude, longitude and altitude over observation site, the minimum and maximum radii of aerosol particles, and the assumed refractive index for each wavelength (Nakajima et al., 1996). Then the aerosol optical depth, size distribution, single scattering albedo and refractive index can be retrieved from the observation of direct and scattering solar irradiances, as well as aureole radiances. Its structure and inversion accuracy are discussed in detail in the literature (Nakajima et al., 1996; Tonna et al., 1995). And on an average, the errors for the minimum and maximum size ranges (0.05–0.1 μm and 7–15 μm) may be as large as 35–100%, but the precision for the middle range is expected to be larger than 80%.

The Angstrom exponent is determined from the spectral dependence of the measured optical depth, and is a good indicator of the aerosol size. This coefficient is

computed using the regression analysis, in which the AOD values for three wavelengths (400, 500 and 675 nm) are fitted to the following equation:

$$\tau_a(\lambda) = \beta\lambda^{-\text{alpha}}, \quad (1)$$

where λ is the wavelength, and β is the aerosol turbidity coefficient (AOD at $\lambda = 1$ μm). The data for ALPHA are used only when a good correlation coefficient ($R > 0.90$) is obtained in the regression analysis using Eq. (1).

The radiometer automatically collects data regarding of sky conditions (except for rainy conditions) according to a preprogrammed sequence, thus, the cloud screening is essential for data quality purpose. Here, the cloud screening method developed by Smirnov et al. (2000) and applied to AERONET data was utilized. This technique is based on the principle that clouds have larger optical depths and greater temporal variances than do aerosols. In addition, manual cloud screening for questionable data was performed using weather observations from the Yinchuan observatory.

The aerosol radiative forcing (ARF) at the top of the atmosphere (TOA) and at the surface is defined as the difference in the net fluxes (down minus up) (solar plus long wave; in W m^{-2}) with and without aerosol at the TOA and at the surface levels, respectively. And the aerosol direct radiative forcing efficiency is defined as the ratio between the ARF value and its corresponding AOD value (Xia et al., 2005). To carry out the radiative forcing computations we have used the Santa Barbara DISORT Atmospheric Radiative Transfer (SB-DART) model (Ricchiazzi et al., 1998), which is developed by the atmospheric science community, and is a discrete ordinates radiative transfer model (Stamnes et al., 1988). It is being used widely for the radiative transfer calculations. This algorithm includes multiple scattering in a vertically inhomogeneous nonisothermal plane-parallel media, and it has been shown to be computationally efficient and to reliably resolve the radiative transfer equation. The main input data consists of the solar zenith angle, where you have the opinion of specifying a particular solar zenith angle or enter a particular date, time, latitude and longitude to calculate the solar zenith angle using one small code in the SB-DART; the spectrum range of calculating fluxes, where you can choose the shortwave (0.25–4.0 μm), long wave (4.0–100 μm) and entire spectrum (0.25–100 μm); atmospheric profile (nine standard); the trace gases including CO_2,CH_4 and N_2O (the default values or any input values.); the surface albedo model (six different surfaces you can choose or input your own value); the aerosol parameters, where you can choose no aerosols or one special aerosol model from four models and input the AOD550 nm; the cloud parameters and the parameters what you want to obtain. The output data for each run include down flux, up flux, direct flux and net flux for the entire atmospheric column or down flux, up flux, direct flux at which point in the atmospheric column (top or bottom) for the ten variables, including hour of day, solar zenith angle, wavelength, ect at the given range and step. The overall uncertainty in the estimated forcing due to deviations in simulation is found in the range 10–15%. And the detailed discussion about this model is in the literature (Ricchiazzi et al., 1998). In our study, we calculated the down radiative flux and up radiative flux at the surface and TOA for the variable wavelength ranging from 0.25 μm to 4.0 μm with a step of 0.25 μm, under the aerosol present and not. Then the radiative forcing efficiency was estimated at the surface and TOA at the 0.25–4 μm. The solar zenith angles have used the seasonal average value. And based upon the geographical location, measured parameters and the prevailing weather conditions, we have used the mid-latitude summer atmospheric profile for spring, summer and autumn and the mid-latitude winter atmospheric profile for winter, and have used the default value of trace gases and the urban aerosol model. The $AOD_{550\ nm}$ value is determined from the value of $AOD_{500\ nm}$ using the power law as follows:

$$AOD_{550\ nm} = AOD_{500\ nm}(550/500)^{-\text{alpha}},$$

where alpha is the Angstrom exponent (400–675 nm) (Prasad et al., 2007).

4. Results and discussion

4.1. Aerosol optical depth and Angstrom exponent

The AOD is representative of the airborne aerosol loading in the atmospheric column and is important for the identification of aerosol source regions and aerosol evolution. Fig. 1 shows the monthly mean aerosol optical depth at 500 nm from October 2003 to August 2004, with error bars showing the standard deviation of the monthly averaged value. The mean AOD varies on a monthly basis with the smallest values occurring from October to February with a minimum in February (0.175±0.019), indicating that the atmosphere was relatively clean during this period. According to the data of Chinese duststorm net (http://www.duststrom.com.cn), there were total fourteen dust events in 2004, and most of those occurred in spring. Due to the influence of these dust activities, the AOD increased from March to May, reaching its maximum value in May (0.398±0.028). The mean

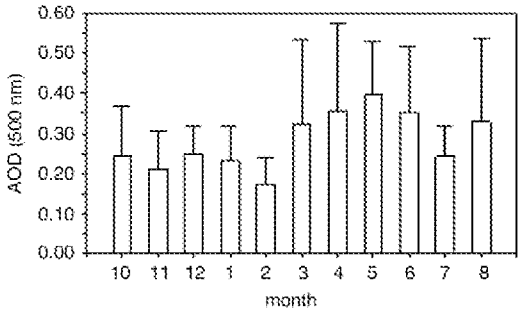

Fig. 1. Monthly average aerosol optical depth (500 nm) and standard deviation.

AOD in June and August was a little lower than that in May, but was also high, reflecting the influence of resident atmospheric dust particles after dust activities (in June) and local meteorological conditions, such as high temperature (Lyamani et al., 2006a), and pollutant particles (in August). The relatively lower mean AOD in July was due to wash-out by rainfall events. Generally speaking, the AOD values were smaller in fall and winter and bigger in spring and summer. Liu et al. (2004) found that AOD values were smaller in summer and fall and bigger in winter and spring, based on spectrophotometer data collected at Yinchuan in 2002. This illustrates how AOD can vary over time and is influenced by climatic conditions. Fig. 2 is the monthly mean ALPHA (400–675 nm), and its standard deviation. On the whole, the change in ALPHA was opposite to that of AOD. The smallest ALPHA values appeared in March to May, which indicates that the aerosol particles were large during this period and likely related to dust activities. Smaller aerosol particles appear to dominate during November to January and in July. ALPHA and AOD values were high in August, which indicates that there was an increase in the contribution of fine particles during this high temperature period (Lyamani et al., 2006a). ALPHA values were always greater than 0.5 except during March and April, which signifies the greater contribution of fine particles to extinction over the Yinchuan region.

Diurnal variability of aerosol optical depth is important for various applications, including satellite aerosol data validation, radiative forcing computations, studies of aerosol interaction with humidity and clouds, and also public health (Kaufman, 2001; Smirnov, 2002). At most urban/industrial AERONET sites, a prevailing pattern of the AOD was shown to increase by 10–40% during the daytime and the dust aerosol could not be generalized a diurnal trend (Smirnov, 2002). Fig. 3 shows the diurnal variability of aerosol optical depth at a wavelength 500 nm. All individual observations for a day are expressed as a percentage departure from the daily mean. Computed percentages were averaged hourly (0300–0400 GMT, 0400–0500 GMT etc.) for each measurement period. The sampling procedure, which is similar to one used by Peterson et al. (1981), renders systematic diurnal trends more evident. The diurnal variability of AOD in Yinchuan was significant, and its variety about 31%, 33%, 24% and 38% in spring, summer, autumn and winter, respectively. AOD steadily increased in the morning, reaching the maximum value and then decreased dramatically in spring, summer and autumn, and the only difference was the time of maximum in each season. But, in winter, AOD increased first, reaching the maximum at 13:00 pm and then decreased, but increased again from 15:00 pm. Smirnov et al. (2002) and Xia et al. (2006) found that the AOD steadily increased throughout the daytime and reaches maximum in the late afternoon for the most urban/industrial areas, including in Beijing, located in north of China. This difference is mainly due to the different composing of aerosol and climatic conditions.

Some studies have pointed that the accurate statistic characterization of AOD can accurately search for one appropriate parameterization which is as simple as possible

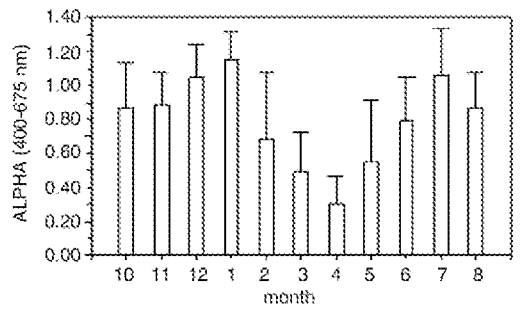

Fig. 2. Monthly average Angstrom exponent (400–675 nm) and standard deviation.

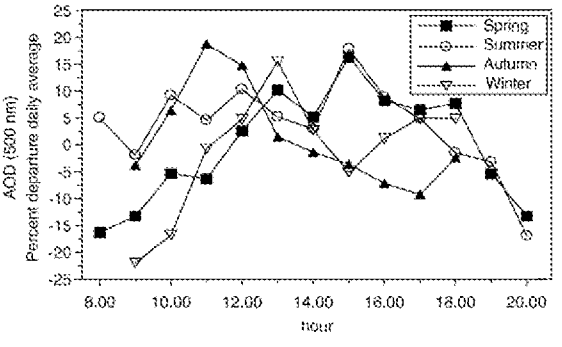

Fig. 3. Diurnal variability of AOD computed hourly as percent departure from daily average.

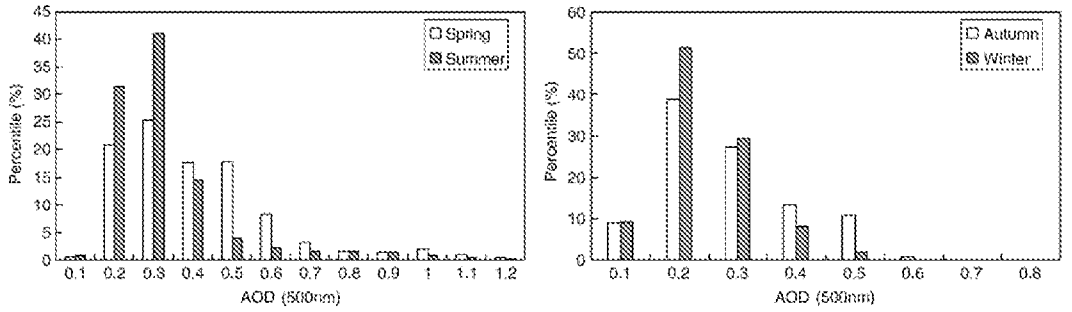

Fig. 4. The frequency distributions of AOT (500 nm) for each season in Yinchuan (left: spring and summer; right: autumn and winter).

while achieving a level of distribution characterization which contents to the accuracy needs of model driven applications such as radiative forcing or aerosol dispersion, and also tell us something more about the variations of natural phenomena (O'Neill et al., 2000). Previous studies have shown that the frequency distribution of AOD, τ, can be described by the following log-normal distribution:

$$f(\tau) = \frac{1}{s\tau\sqrt{2\pi}} \exp\left(\frac{(\ln \tau - m)^2}{2s^2}\right);$$

this means that $\ln\tau$ follows a Gaussian (or normal) distribution with mean, m, and the standard deviation, s (O'Neill et al., 2000; Matthias and Bosenberg, 2002; Behnert et al., 2007). Figs. 4 and 5 show the frequency distributions of AOD (500 nm) and ALPHA (400–675 nm) for each season. Apart from the data of influenced by cloud, the number statistics of samples is 1292, 1486, 1443 and 1492 in spring, summer, autumn and winter, respectively. Based on results from spring and summer, it is more suitable to depict AOD frequency distributions by the log-normal probability distribution than by a normal probability distribution, which is consistent with O'Neill et al. (2000). The normal probability distribution was found to better represent ALPHA frequency distributions (O'Neill et al., 2000; Nwofor et al., 2007), especially in summer in our study. Fig. 4 shows that approximately 81% of the AODs ranged between 0.1 and 0.5 and that 55% of the AODs ranged between 0.3 and 0.5 in spring; about 72%, 66% and 80.8% varied between 0.1 and 0.3 in summer, autumn and winter, respectively. Especially in winter, nearly 51.5% of the AODs varied between 0.1 and 0.2. From Fig. 5, nearly half of the ALPHA values were smaller than 0.5 in spring and about 58.7% of the values varied between 0.7 and 1.1 during the summer. More than 76% of the ALPHA values ranged between 0.7 and 1.3 in autumn and approximately 68% of the values were larger than 0.9 in winter.

The dependence of ALPHA on aerosol optical depth was used by Fouquart et al. (1987) and D'almeida (1987) to obtain the aerosol size distribution. Xia et al. (2004) found that the relationship between ALPHA and AOD at 500 nm for four seasons at Dunhuang (DH) showed a similar dependence of ALPHA on AOD. Cheng et al. (2006a) also studied this relationship at five sites in China: Dunhuang (DH), Yulin (YL), Beijing (BJ), Xianghe (XH), Inner_Mongolia (IM) and Liaoning (LN). The results showed that since the DH, YL and IM sites were located near dust sources, aerosol loading mainly consisted of dust particles, and that the relationship between ALPHA and

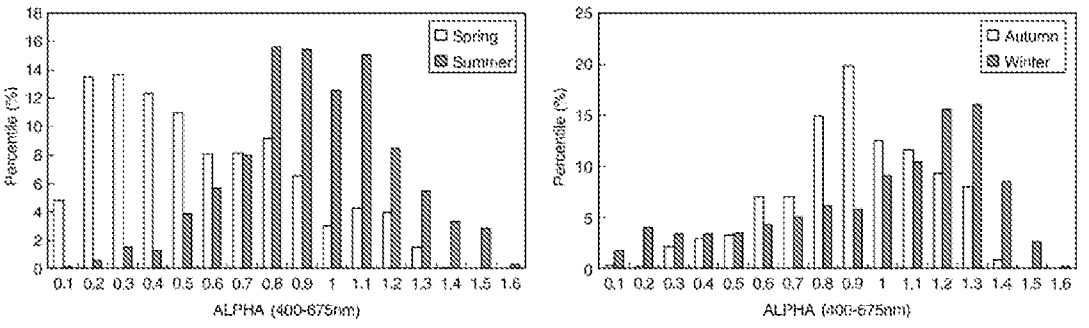

Fig. 5. The frequency distributions of ALPHA (400–675 nm) for each season in Yinchuan (left: spring and summer; right: autumn and winter).

AOD could be characterized by an integrated exponential function. The BJ, XH and LN sites showed a more complex scenario, especially at the BJ and LN sites. Fig. 6 shows the scatterplots of instantaneous ALPHA as a function of AOD at 500 nm for each season in Yinchuan. An exponential dependence of ALPHA on AOD in spring is suggested, which is similar to results reported by Xia et al. (2004) for the DH site and Cheng et al. (2006a) for the DH, YL and IM sites. There is no obvious relationship between ALPHA and AOD for the other seasons, this behavior was also noted by Cheng et al. (2006a) for the BJ and LN sites. And this can be explained by the predominance of dust particles with larger size and the aerosol source is relative singleness in spring, and the combined contribution of dust and pollutant particles with different rate of various aerosol loading and the aerosol source is relative complexity in other seasons. It indicated that the main sources of aerosol in Yinchuan varied with different seasons. Cheng et al. (2006a) pointed out that this variation of the relationship between ALPHA and AOD might provide a possible way to identify and estimate the effects of different sources on aerosol loading and aerosol size.

4.2. Aerosol size distribution

The relationship between aerosol size distribution and AOD is important for studying aerosol climate forcing. The aerosol size distribution was determined using 20 radius size bins between 10^{-6} cm–2×10^{-3} cm. For each month, the average radius of aerosol particles in each bin was calculated. Fig. 7 illustrates the monthly variation in aerosol size. The aerosol size distribution has a two-mode structure, which can be characterized by the sum of two log-normal distributions as follows:

$$v(r)=\frac{dV(r)}{d\ln r}=\sum_{i=1}^{2}\frac{C_{v,i}}{\sqrt{2\pi}\sigma_i}\exp\left[-\frac{(\ln r-\ln r_{v,i})}{\sigma_i^2}\right],$$

where $r_{v,i}$ is the volume median radius, σ_i is the standard deviation, and $C_{v,i}$ is the volume concentration for accumulation and coarse modes. These integrated quantities can be approximated according to Dubovik et al. (2002). There is one accumulation mode with a radius about 0.15 μm, which shows a steady monthly variation and a maximum value in August; this is mainly related to human activities and meteorological conditions. A coarse mode with a radius of about 7 μm is evident, as are the large variations over the months; this reflects the influence of dust events. There was little change in the particle volume median radius during dust and non-dust periods, only changes in particle concentration. During the dust episodes, the coarse particle concentration in the atmosphere was about 2–3 times more than that during periods when there was no dust activity. The average volume

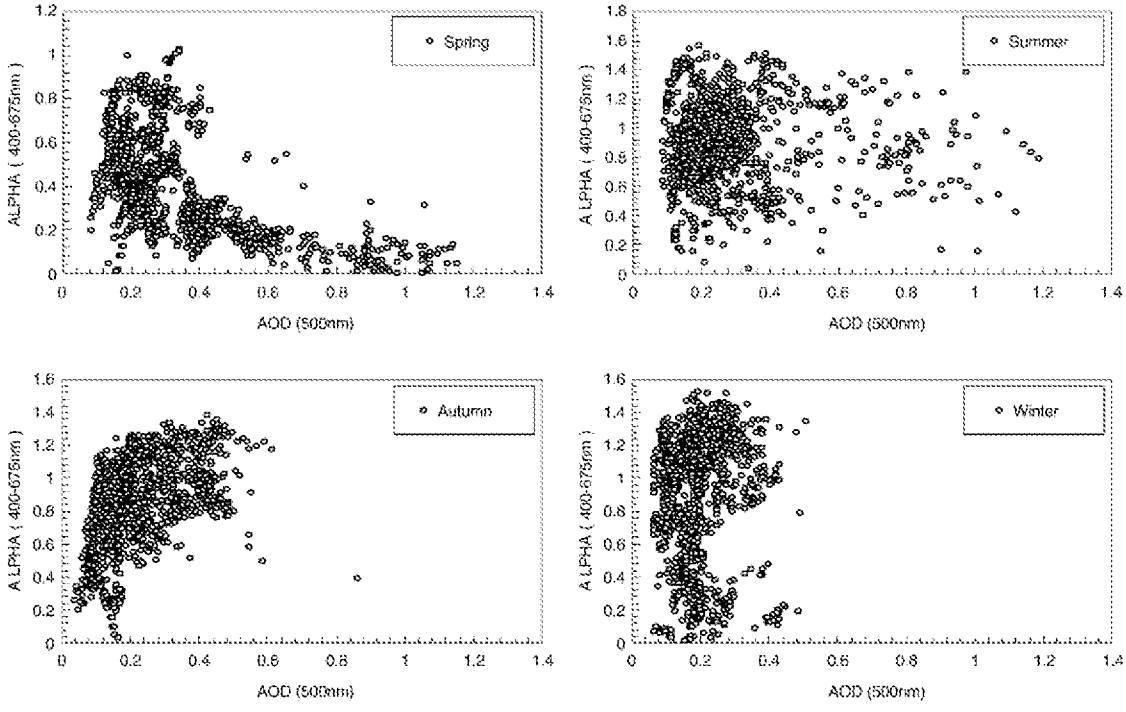

Fig. 6. The scatter plots of instantaneous ALPHA as a function of AOT at 500 nm for each season.

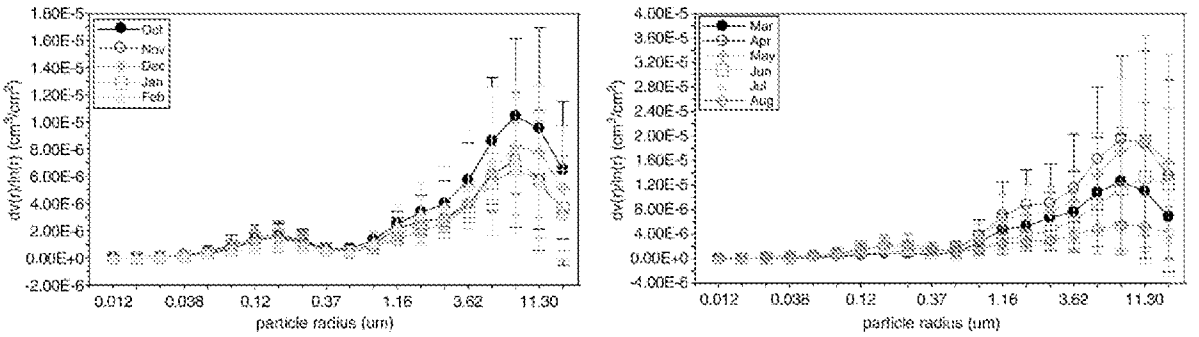

Fig. 7. Monthly average of aerosol volume spectrum (500 nm) at 20 different radiuses and standard deviation (left: Oct–Feb; right: Mar–Aug).

spectrum of large particles (defined as particles with radii larger than 0.5 μm) was calculated and is equal to $6.03\times10{-}6$ cm^3/cm^2; for smaller particles, the average volume spectrum is 6.57×10^{-7} cm^3/cm^2. The former is more than 9 times greater than the latter, which indicates that the coarse particle concentration was high throughout the year over the Yinchuan area.

The number of particles in the accumulation mode was greater in August than in April and vice-versa for the coarse mode. Given that the mean AOD values for these two months are similar, the extinction capability of the accumulation mode aerosol was more than that of the coarse mode aerosol (Zhang et al., 2004).

4.3. Refractive index

The greatest information about the refractive index comes from aureole radiances, which are strongly affected by errors in the angle-pointing bias. And some studies carefully discussed the refractive index determination of atmospheric aerosol particles by ground-based solar extinction and scattering measurements (Wendisch et al., 1994; Nakajima, 1996). The errors are estimated to be ±0.04 in the real parts of the refractive index and 50% in the imaginary parts of the refractive index. Fig. 8 shows the monthly average of the real parts of the aerosol refraction index at 400, 500, 675, 870 and 1020 nm. There is no remarkable variation of the real parts of the refractive index at the different wavelengths. This low sensitivity to wavelengths varied slightly with time, but no clear pattern was found. The average value of the real part of the refractive index at the 3 highest wavelengths (675, 870, and 1020 nm) is 1.5288 while the average value at the 2 lower wavelengths (400 and 500 nm) is 1.5099. This may be due to the appearance of large amounts of coarse particles, resulting in a relatively higher absorption in the near-infrared than in the visible (Yu et al., 2006). Over the study period, the monthly averaged real part of the refractive index ranged from 1.47 to 1.55 with a mean value of 1.51. Given that the real part of the refractive index of dust aerosols is greater than that of anthropogenic aerosols and that the largest values appear in spring, the influence of dust events over this area during this season is apparent.

Fig. 9 shows the monthly averaged imaginary parts of the aerosol refraction index at 5 wavelengths. Similar to the real parts of the refractive index, the imaginary parts also show a low sensitivity to wavelength. These results are consistent with the computed values of the imaginary parts of the refractive index found in the literatures (Yu et al., 2006; Cheng et al., 2006a,b). This low sensitivity of the imaginary parts of the refractive index to wavelength also varied slightly with time. The largest values of the imaginary part of the refractive index are found at 400 nm. The imaginary parts of the refractive index decreased slightly between 400 and 675 nm and then increased a bit more between 675 and1020 nm. The average values of the imaginary parts of the refractive index at each wavelength were 0.0108, 0.0095, 0.0079, 0.0087 and 0.0098 at 400, 500, 675, 870 and 1020 μm, respectively.

The significant seasonal variation of the imaginary part of the refractive index illustrates the influence of

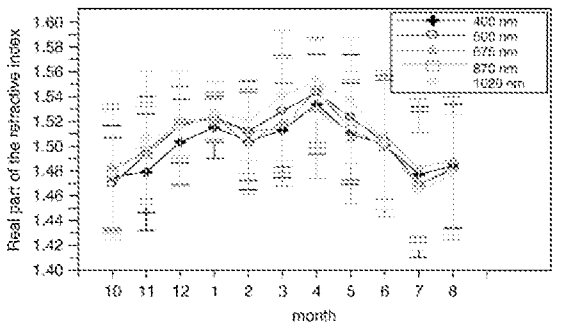

Fig. 8. Monthly averaged real part of aerosol complex refraction index and standard deviation.

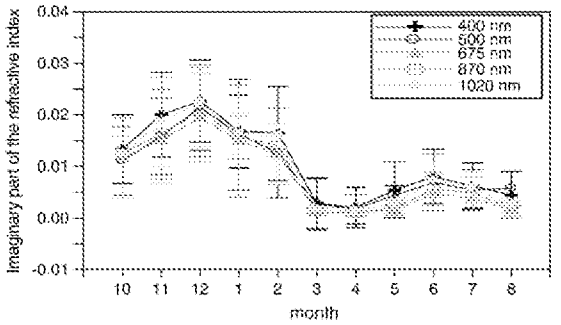

Fig. 9. Monthly averaged imaginary part of aerosol complex refraction index and standard deviation.

different aerosol components over the Yinchuan region. The largest average value of the imaginary part of the refractive index (0.016) appears in winter, while the smallest average value (0.002) is seen during the spring. The above results indicate that dust activities might affect aerosol radiative effects through the input of large volumes of dust aerosols, and also through their effects on aerosol's physical and radiative properties.

4.4. Single scattering albedo

The single scattering albedo, ω_o, is a common measurement of the relative contribution of absorption to extinction and is a key variable in assessing the climatic effects of aerosols (Jacobson, 2000; Dubovik et al., 2002). Its value is mostly dependent on the composition matters and size distribution of aerosol particles. The single scattering albedo of desert dust simulated according to a number of models (Shettle and Fenn, 1979; WMO, 1983; Koepke et al., 1997; Hess et al., 1998) ranges from 0.63 to 0.87 at 500 nm, while aircraft radiation measurements (Fouquart et al., 1987) suggest lower absorption (ω_o=0.95 for the broadband solar spectrum). And the main source of error in the derived single scattering albedo is due to calibration of the sky data, and is estimated to be ±0.03.

Table 1 shows the monthly average single scattering albedo and corresponding standard deviations at 400, 500, 675, 870 and 1020 nm. Due to the accuracy of inversion is decreasing with low AOD, only data corresponding to AOD lager than 0.3 have been used to statistic. In spring, due to the influence of dust events, the scattering contribution of coarse particles was increased, and the single scattering albedo showed a slight increasing trend with wavelength (Dubovik et al., 2002; Xia et al., 2005; Cheng et al., 2006b). The single scattering albedo in spring was much higher than that in other seasons, with an average value of 0.94±0.02 at 500 nm. This is lower than single scattering albedo values obtained by others for desert dust (0.95–0.99) (Dubovik et al., 2002; Kaufman et al., 2001), which suggests the possible combination of dust, urban/industrial particles and biomass burning aerosols over the Yinchuan area. In other seasons, the single scattering albedo decreased with wavelength. But compared with other studies, this trend was not dramatic, approximately decreased 0.4 from 400 nm to 1020 nm. Lyamani et al. (2006b) once found that in air masses over Europe and the Mediterranean, the single scattering albedo decreased sharply with wavelength from 0.91±0.02 at 440 nm to 0.83±0.04 at 1020 nm. So the variation of single scattering albedo with wavelength has regional characteristics.

4.5. Aerosol direct radiative forcing

The important aerosol optical properties and aerosol load can produce a significant impact on aerosols' radiative forcing (ARF) and significantly alter the radiative balance over the region. In our study, the direct radiative forcing efficiency at surface and TOA at the shortwave range were estimated using the SB-DART

Table 1
Monthly averaged single scattering albedo and corresponding standard deviations

	400 nm	500 nm	675 nm	870 nm	1020 nm
Oct	0.89±0.02	0.87±0.01	0.87±0.02	0.85±0.02	0.85±0.03
Nov	0.87±0.01	0.87±0.02	0.85±0.02	0.84±0.02	0.83±0.03
Dec	0.85±0.01	0.83±0.02	0.83±0.02	0.82±0.03	0.80±0.02
Jan	0.85±0.01	0.84±0.01	0.83±0.02	0.82±0.01	0.81±0.03
Feb	0.87±0.01	0.84±0.01	0.85±0.01	0.85±0.02	0.86±0.02
Mar	0.93±0.02	0.95±0.02	0.95±0.02	0.96±0.01	0.98±0.02
Apr	0.91±0.02	0.92±0.02	0.93±0.02	0.95±0.02	0.96±0.02
May	0.92±0.02	0.95±0.02	0.95±0.02	0.96±0.02	0.97±0.03
Jun	0.91±0.02	0.91±0.02	0.88±0.02	0.88±0.03	0.90±0.03
Jul	0.89±0.02	0.87±0.02	0.85±0.03	0.85±0.02	0.83±0.02
Aug	0.89±0.01	0.86±0.01	0.85±0.02	0.84±0.01	0.83±0.02

Table 2
Aerosol direct radiative forcing efficiency for each season

	Spring	Summer	Autumn	Winter
Surface ($W \cdot m^{-2}$)	−055.31	−59.71	−60.13	−60.38
TOA ($W \cdot m^{-2}$)	13.89	10.39	2.30	2.64

model. The assumptions of the input parameters have been given in Section 3. Table 2 shows the aerosol direct radiative forcing efficiency for each season over Yinchuan area. In spring, the aerosol direct radiative forcing efficiency value at surface/TOA is lower/higher than that in other seasons, and these results are similar to the computed values of the aerosol's direct radiative forcing efficiency found in the literatures (Xia et al., 2005; Prasad et al., 2007). The reason is mainly due to the influence of Asian dust activities in spring, the net radiation at surface increased and the return to the top of the atmosphere of radiation also enhanced. And thus, the atmospheric radiation absorption rate decreased. And the direct radiative forcing efficiency value at the shortwave range is −55.31, −59.71, −60.13 and −60.38 at surface and 13.89, 10.39, 2.30 and 2.64 at TOA in spring, summer, autumn and winter, respectively.

5. Summaries

The aerosol optical depth (AOD), Angstrom wavelength exponent (ALPHA), volume size distributions, refraction index and single scattering albedo over Yinchuan, a city in northwest China, were retrieved using the data of sky radiometer from October 2003 to August 2004.

The AOD over the Yinchuan area varies with season, with a vernal maximum and a winter minimum, and is mainly influenced by weather conditions, dust events and human activities. The magnitude of ALPHA was relatively high throughout the year, indicating the greater contribution of fine particles to extinction in the region; the highest values were seen in winter and the smallest values appeared in spring. The diurnal variability of AOD in Yinchuan varied about 31%, 33%, 24% and 38% in spring, summer, autumn and winter, respectively, and showed a similar variation pattern in spring, summer and autumn and had another variation pattern in winter. The frequency distribution of AOD and ALPHA approximately follows a log-normal distribution and a normal probability distribution, respectively. In the spring, approximately 81% of the AODs ranged between 0.1 and 0.5 and 55% of the AOD_S ranged between 0.3 and 0.5; about 72%, 66% and 80.8% varied between 0.1 and 0.3 in summer, autumn and winter, respectively. The magnitudes of nearly half of the ALPHA values were smaller than 0.5 in spring and about 58.7% of the values ranged between 0.7 and 1.1 in summer; in autumn and winter, about 76% of the values varied between 0.7 and 1.3 and approximately 68% of the values were larger than 0.9, respectively. The relationship between ALPHA and AOD shows a simple dependence of ALPHA on AOD in spring and can be characterized by one integrated exponential function. No clear dependence of ALPHA on AOD was evident in other seasons, indicating that the main sources of aerosol in Yinchuan varied with season.

The aerosol volume size distribution can be characterized by the sum of two log-normal distributions, and has two modes: an accumulation mode with a radius of 0.15 μm (maximum in August), and a coarse mode with a radius of 7 μm (maxima in April and May).

The real and the imaginary parts of the refraction index are clearly affected by dust events, with the real parts increasing in spring and the imaginary parts decreasing in spring. Both real and imaginary parts of the refractive index are not sensitive to wavelength although a slight variation with time was noted. The real parts of the refractive index were generally higher at the near-infrared wavelengths (average value = 1.5288) than at the visible wavelengths (average value = 1.5099). The magnitude of the imaginary part of the refractive index decreased slightly between 400 and 675 nm and then increased between 675 and 1020 nm.

The single scattering albedo in spring was clearly higher than in other seasons and showed a slight increasing trend with wavelength. In other seasons, the single scattering albedo decreased with wavelength. The variation of single scattering albedo with wavelength has regional characteristics, which is corroborated by other studies. The single scattering albedo values obtained in spring are lower than those reported by others for desert dust (0.95–0.99), which suggests the possible combination of dust, urban/industrial particles and biomass burning aerosols over Yinchuan.

Regarding the aerosol radiative effects over Yinchuan area, the aerosol direct radiative forcing efficiency value at surface/TOA in spring is lower/higher than in other seasons. The value of it is −55.31, −59.71, −60.13 and −60.38 at surface and 13.89, 10.39, 2.30 and 2.64 at TOA in spring, summer, autumn and winter, respectively.

Acknowledgments

This work was supported by the National Basic Research Program of China (2006CB403705). We thank Prof. Guangyu Shi, Institute of Atmospheric Physics, Chinese Academy of Sciences, for providing the direct and scattering solar irradiance data from Yinchuan. We are grateful to the OpenCLASTR project for use of their 'SKYRAD' package in this research. We also thank Maki Yamano, Center for Climate System Research, University of Tokyo, for her help in the running of the code.

References

Bates, T.S., Anderson, T.L., Baynard, T., Bond, T., Boucher, O., Carmichael, G., et al., 2006. Aerosol direct radiative effects over the northwest Atlantic, northwest Pacific, and North Indian Oceans: estimates based on in situ chemical and optical measurements and chemical transport modeling. Atmospheric chemistry Physical Discussion 6, 175–362.

Behnert, I., Matthias, V., Doerffer, R., 2007. Aerosol climatology from ground-based measurements for the southern North Sea. Atmospheric Research 84, 201–220.

Chen, Y., Lohmann, U., Zhang, J., Luo, Y., Liu, Z., Lesins, G., 2005. Contribution of changes in sea surface temperature and aerosol loading to the decreasing precipitation trend in Southern China. Journal of Climate 18 (9), 1381–1390.

Cheng, T., Wang, H., Xu, Y., Li, H., Tian, L., 2006a. Climatology of aerosol optical properties in northern China. Atmospheric Environment 40, 1495–1509.

Cheng, T., Liu, Y., Lu, D., Xu, Y., Li, H., 2006b. Aerosol properties and radiative forcing in Hunshan Dake desert, northern China. Atmospheric Environment 40, 2169–2179.

D'almeida, G.A., 1987. On the variability of desert aerosol radiative characteristics. Journal of Geophysical Research 92, 3017–3026.

Dubovik, O., Holben, B., Eck, T.F., Smirnov, A., Kaufman, Y.J., et al., 2002. Variability of absorption and optical properties of key aerosol types observed in worldwide locations. Journal of the Atmospheric Sciences 59, 590–608.

Fouquart, Y., Bonnel, B., Brgniez, J.C., et al., 1987. Observation of Saharan aerosols: results of ECLATS Field experiment: II. Broadband radiative characteristics of the aerosols and vertical radiative flux divergence. Journal of climate and Meteorology 25, 38–52.

Hansen, J., Sato, M., Ruedy, R., Lacis, A., Oinas, V., 2000. Global warming in the twenty-first century: an alternative scenario. Proceedings of the National Academy of Sciences of the United States of America 97, 9875–9880.

Hess, M., Koepke, P., Schult, I., 1998. Optical properties of aerosol and clouds: the software package OPAC. Bulletin of the American Meteorological Society 79, 831–844.

Holben, B.N., Kaufman, Y.J., Eck, T.F., Slutsker, I., Tanre, D., et al., 1998. AERONET—a federated instrument network and data archive for aerosol characterization. Remote Sensing of Environment 66, 1–16.

Holben, B.N., Tanre, D., Smirnov, A., Eck, T.F., Slutsker, I., Abuhassan, N., et al., 2001. An emerging ground-based aerosol climatology: aerosol optical depth from AERONET. Journal of Geophysical Research 106, 12,067–12,097.

IPCC, 2001. Climate change 2001. The Scientific Basis—Contribution of Working Group I to the Third Assessment Report of the Intergovernmental Panel on Climate Change. Cambridge University Press, New York.

IPCC, 2007. Climate change 2001 the scientific basis. In: Solomon, S., Qin, D., Manning, M., et al. (Eds.), Contribution of Working Group I to the Forth Assessment Report of the Intergovernmental Panel on Climate Change. Cambridge University Press, Cambridge, United Kingdom and New York, NY, USA.

Jacobson, M.Z., 2000. A physically-based treatment of elemental carbon optics: implications for global direct forcing of aerosols. Geophysical Research Letter 27, 217–220.

Kaufman, Y.J., Tanre, D., Boucher, O., 2002. A satellite view of aerosols in the climate system. Nature 419, 215–223.

Kaufman, Y.J., Tanre, D., Dubovik, O., Karnieli, A., Remer, L.A., 2001. Absorption of sunlight by dust as inferred from satellite and ground-based remote sensing. Geophysical Research Letters 28 (8), 1479–1482.

Kelly, J.T., Chuang, C.C., Wexler, A.S., 2007. Influence of dust composition on cloud droplet formation. Atmospheric Environment 41, 2904–2916.

Koepke, P., Hess, M., Schult, I., et al., 1997. Global aerosol data set. MPI Meteorologie Hamburg Rep., 243, p. 44.

Liu, Y., Niu, S., Zheng, Y., 2004. Optical depth characteristics of Yinchuan atmospheric aerosols based on the CE-318 sun tracking spectrophotometer data. Journal of Nanjing Institute of Meteorology 27 (5), 615–622.

Lyamani, H., Olmo, F.J., Alcantara, A., Alados-Arboledas, L., 2006a. Atmospheric aerosols during the 2003 heat wave in southeastern Spain I: spectral optical depth. Atmospheric Environment 40, 6453–6464.

Lyamani, H., Olmo, F.J., Alcantara, A., Alados-Arboledas, L., 2006b. Atmospheric aerosols during the 2003 heat wave in southeastern Spain II: microphysical columnar properties and radiative forcing. Atmospheric Environment 40, 6465–6476.

Mao, J., Li, C., 2006. Observation study of aerosol radiative properties over China. Acta Meteorlogica Sinica 20 (3), 306–321.

Matthias, V., Bosenberg, J., 2002. Aerosol climatology for the planetary boundary layer derived from regular lidar measurements. Atmos. Res. 63, 221–245.

Nakajima, T., Tonna, T., Rao, R., Boi, P., Kaufman, Y.J., Holben, B., 1996. Use of sky brightness measurements from ground for remote sensing of particulate polydispersions. Applied Optics 35, 2672–2686.

Nwofor, O.K., Chidiezie Chineke, T., Pinker, R.T., 2007. Seasonal characteristics of spectral aerosol optical properties at a sub-Saharan site. Atmospheric Chemistry 85 (1), 38–51.

O'Neill, N.T., Miller, J.R., 1984. Combined solar aureole and solar beam extinction measurements. I: calibration considerations. Applied Optics 23, 3691–3696.

O'Neill, N.T., Ignatov, A., Holben, B.N., Eck, T.F., 2000. The lognormal distribution as a reference for reporting aerosol optical depth statistics; empirical tests using multi-year, multi-site AERONET sunphotometer data. Geophys. Res. Lett. 27 (20), 3333–3336.

Osborne, S.R., Haywood, J.M., Francis, P.N., Dubovik, O., 2004. Short-wave radiative effects of biomass burning aerosol during SAFARI2000. Q.J.R. Meteorology Society 130, 1423–1448.

Peterson, J.T., Flowers, E.C., Berri, G.J., Reynolds, C.L., Rudisill, J.H., 1981. Atmospheric turbidity over central North Carolina. Journal of Applied Metalworking 20, 229–241.

Prasad, A.K., et al., 2007. Aerosol radiative forcing over the Indo-Gangetic plains during major dust storms. Atmospheric Environment. doi:10.1016/j.atmosenv.2007.03.060.

Ricchiazzi, P., Yang, S.R., Gautier, C., Sowle, D., 1998. SBDART: a research and teaching software tool for plane-parallel radiative transfer in the Earth's atmosphere. Bulletin of the American Meteorological Society 79 (10), 2101–2114.

Schmid, B., Spyak, P.R., Biggar, S.F., Wehrli, C., Sekler, J., Ingold, T., et al., 1998. Evaluation of the applicability of solar and lamp radiometric calibrations of a precision sun photometer operating between 300 and1025 nm. Applied Optics 37, 3923–3941.

Shettle, E.P., Fenn, R.W., 1979. Models of aerosols of lower troposphere and the effect of humidity variations on their optical proprieties. AFCRL Tech. Rep. 79 0214. Air Force Cambridge Research Laboratory, Hanscom Air Force Base, MA, p. 100.

Smirnov, A., Holben, B.N., Eck, T.F., Dubovik, O., Slutsker, I., 2000. Cloud screening and quality control algorithms for the AERONET data base. Remote Sensing of Environment 73, 337–349.

Smirnov, A., Holben, B.N., Eck, T.F., Slutsker, I., Chatenet, B., Pinker, R.T., 2002. Diurnal variability of aerosol optical depth observed at AERONET (Aerosol Robotic Network) sites. Geophysical Research Letters 29 (23), 2115. doi:10.1029/2002GL016305.

Stamnes, K., Tsay, S.C., Wiscombe, W., Jayaweera, K., 1988. Numerically stable algorithm for discrete–ordinate-method radiative-transfer in multiple-scattering and emitting layered media. Applied Optics 27 (12), 2502–2509.

Takamura, T., Nakajima, T., Okada, I., Uchiyama, A., Sugimoto, N., Shi, G., Zhou, J., 2002. Aerosol Cloud-radiation Study Using the SKYNET Data. The first ADEC Workshop, Tokyo, Japan. http://www.aeoliandust.com.

Tanaka, M., Nakajima, T., Shiobara, M., 1986. Calibration of a sunphotometer by simultaneous measurements of direct-solar and circumsolar radiations. Applied Optics 25, 1170–1176.

Tonna, G., Rao, R., Nakajima, T., 1995. Aerosol features retrieved from solar aureole data: a simulation study concerning a turbid atmosphere. Applied Optics 34, 4486–4499.

Wang, H., Shi, G., Aeruo, A., Wang, B., Zhang, T., 2004. Radiative forcing due to dust aerosol over east Asia–north Pacific region during spring, 2001. Chinese Science Bulletin 49 (20), 2212–2219.

Wendisch, M., Hoyningen-Huene, W., 1994. Possibility of refractive index determination of atmospheric aerosol particles by ground-based solar extinction and scattering measurements. Atmospheric Environment 28 (5), 785–792.

WMO, 1983. Radiation commission of IAPAM meeting of experts on aerosol and their climatic effects. World Meteorological Organisation Rep. WCP55, 28–30.

WMO, 2001. Strategy for the implementation of the global atmosphere watch programme (2001~2007). WMO No. 142. World Meteorological Organization, Geneva, pp. 43–45.

Xia, X., Chen, H., Wang, P., 2004. Aerosol properties in a Chinese semiarid region. Atmospheric Environment 38, 4571–4581.

Xia, X., Wang, P., Chen, H., Gouloub, P., Zhang, W., 2005. Ground-based remote sensing of aerosol optical properties over north China in spring. Journal of Remote Sensing 9 (4), 429–437.

Xia, X., Chen, H., Wang, P., Zhang, W., Goloub, P., Chatenet, B., Eck, T., Holben, B., 2006. Variation of column-integrated aerosol properties in a Chinese urban region. Journal of Geophysical Research 111, D05204. doi:10.1029/2005JD006203.

Xin, J., Wang, Y., Li, Z., Wang, P., Hao, W., Nordgern, B., Wang, S., Liu, L., Wen, T., Sun, Y., Hu, B., 2007. AOD and Angstrom parameters of aerosols observed by the Chinese sun hazemeter Network from August to December 2004. Journal of Geophysical Research 112, D05203. doi:10.1029/2006JD007075.

Yu, X., Cheng, T., Chen, J., Liu, Y., 2006. A comparison of dust properties between China continent and Korea, Japan in East Asia. Atmospheric Environment 40, 5787–5797.

Zhang, W., Hu, B., Chen, C., Du, P., Zhang, L., Feng, G., 2004. Scattering properties of atmospheric aerosols over Lanzhou City and applications using an integrating nephelometer. Advances in Atmospheric Science 21 (6), 848–856.